2-1-2023

In vivo editing of the pan-endothelium by immunity evading simian adenoviral vector

Reka Lorincz

Aluet Borrego Alvarez

Christopher J Walkey

Samir A Mendonça

Zhi Hong Lu

See next page for additional authors

Authors

Reka Lorincz, Aluet Borrego Alvarez, Christopher J Walkey, Samir A Mendonça, Zhi Hong Lu, Alexa E Martinez, Cecilia Ljungberg, Jason D Heaney, William R Lagor, and David T Curiel

Biomedicine & Pharmacotherapy 158 (2023) 114189

Contents lists available at ScienceDirect

Biomedicine & Pharmacotherapy

journal homepage: www.elsevier.com/locate/biopha

In vivo editing of the pan-endothelium by immunity evading simian adenoviral vector

Reka Lorincz [a], Aluet Borrego Alvarez [a], Christopher J. Walkey [b], Samir A. Mendonça [a], Zhi Hong Lu [a], Alexa E. Martinez [b], Cecilia Ljungberg [b], Jason D. Heaney [c], William R. Lagor [b], David T. Curiel [a,*]

[a] Department of Radiation Oncology, Biologic Therapeutics Center, Washington University School of Medicine, 660 South Euclid Avenue, Campus box 8224, St. Louis, MO 63110, USA
[b] Department of Molecular Physiology and Biophysics, Baylor College of Medicine, Houston, TX 77030, USA
[c] Department of Molecular and Human Genetics, Baylor College of Medicine, Houston, TX 77030, USA

ARTICLE INFO

Keywords:
Targeted nonhuman adenoviral vector
Selective gene delivery
Gene editing of vascular endothelium

ABSTRACT

Biological applications deriving from the clustered regularly interspaced short palindromic repeats (CRISPR)-Cas9 site-specific nuclease system continue to impact and accelerate gene therapy strategies. Safe and effective in vivo co-delivery of the CRISPR/Cas9 system to target somatic cells is essential in the clinical therapeutic context. Both non-viral and viral vector systems have been applied for this delivery matter. Despite elegant proof-of-principle studies, available vector technologies still face challenges that restrict the application of CRISPR/Cas9-facilitated gene therapy. Of note, the mandated co-delivery of the gene-editing components must be accomplished in the potential presence of pre-formed anti-vector immunity. Additionally, methods must be sought to limit the potential of off-target editing. To this end, we have exploited the molecular promiscuities of adenovirus (Ad) to address the key requirements of CRISPR/Cas9-facilitated gene therapy. In this regard, we have endeavored capsid engineering of a simian (chimpanzee) adenovirus isolate 36 (SAd36) to achieve targeted modifications of vector tropism. The SAd36 vector with the myeloid cell-binding peptide (MBP) incorporated in the capsid has allowed selective in vivo modifications of the vascular endothelium. Importantly, vascular endothelium can serve as an effective non-hepatic cellular source of deficient serum factors relevant to several inherited genetic disorders. In addition to allowing for re-directed tropism, capsid engineering of nonhuman primate Ads provide the means to circumvent pre-formed vector immunity. Herein we have generated a SAd36.MBP vector that can serve as a single intravenously administered agent allowing effective and selective in vivo editing for endothelial target cells of the mouse spleen, brain and kidney.

Data availability: The data that support the findings of this study are available from the corresponding author upon reasonable request.

1. Introduction

In the changing landscape of gene therapies, one of the biggest hurdles is developing innovative approaches to deliver genome-editing machinery such as clustered regularly interspaced short palindromic repeats (CRISPR)-Cas9 system into disease-relevant cells and tissues in vivo. Specifically, delivery systems targeting vascular endothelium in organs beyond the eye and the liver are of great interest to accomplish safe and effective therapeutic strategies for several cardiovascular disorders and inherited genetic disorders (hemophilia, alpha-1 antitrypsin deficiency, mucopolysaccharidoses type I [1–5]. In vivo gene transfer to the endothelial cells (EC) has been challenging for a long time [6]. Both non-viral and viral vector systems have been employed to approach the delivery issue [7,8]. Recent advances such as alternate viral serotypes [9], viral capsid modification [10], including in vivo phage display and peptide libraries [11,12], coating the surface of nanoparticles with polyethylene glycol (PEG) [13], and application of endothelium specific promoters [7,10] leaded to enhanced EC delivery. Nevertheless, there is still a need to seek highly EC-specific delivery platforms and decrease the shortcomings of viral and non-viral vectors.

* Corresponding author.
E-mail address: dcuriel@wustl.edu (D.T. Curiel).

https://doi.org/10.1016/j.biopha.2022.114189
Received 28 November 2022; Received in revised form 21 December 2022; Accepted 28 December 2022
Available online 30 December 2022

In this regard, the recombinant adeno-associated virus (AAV) is a potential viral platform for targeting and editing the vascular endothelium of various organs. Recent studies explored the utility of AAV-CRISPR systems for in vivo genetic screening and editing of functional genes of the brain endothelium such as the vascular endothelial growth factor receptor 2 (Vegfr2), activing receptor-like kinase 1 (Alk1), or cadherin-associated protein beta 1 (β-catenin) [7,14,15]. These studies demonstrated detectable editing in the vascular endothelium either by using endothelium-specific promoter elements or by local injection of the AAV-CRISPR vectors. Nonetheless, current AAV vectors primarily transduces the liver when administered systemically, raising the concern for potential hepatotoxicity in patients. Additionally, vector-integration-related genotoxicity, low transduction efficiency, tissue specificity, neutralizing antibodies against the AAV capsid, and a limited cargo size of ~4.7 kilobases (kb) are field barriers that will require improvements in the course of clinical development [16–18].

On this basis, alternative vectors are being explored to target endothelial cells with more specificity and efficiency [19]. Systemically administered, EC-targeted Ad enables multi-organ vascular access directly to the disease sites or eventually harness ECs to produce therapeutics for several human diseases with the potential to circumvent vector-associated liver toxicity [9,10]. However, intravenous (iv) administration of human Ad5 (hAd5) vector results in cellular and humoral immune responses limiting sustained therapeutic transgene expression from vector, severely compromising vector efficacy in vaccine and gene therapy applications. Several strategies have been developed to evade preexisting human Ad immunity, including modification of Ad capsid and fiber knob, vector pseudotyping, encapsulation, helper-dependent Ads (HD-Ad), serotype switching, and nonhuman Ad vectors [20]. Applications of genetically modified nonhuman adenovirus serotypes such as simian and gorilla could be employed to avoid preexisting immunity-related concerns and simultaneously reserve the multi-bed vascular targeting capacity [9,21]. On this basis, EC-targeted and liver-untargeted nonhuman serotype Ad, in combination with CRISPR/Cas9 system, could provide the technical basis for long-term gene expression in the presence of preformed anti-Ad5 vector immunity, which significantly expands its utility for a full range of inherited serum deficiency disorders.

In this study, we have evaluated one of the nonhuman Ad vectors, the simian (chimpanzee) Ad type, isolate 36 (SAd36) as a gene-transfer vector for this application. Chimpanzee origin Ads have low seroprevalence in human populations and exhibit a similar safety profile to the human Ad5 [22]. The SAd36 has been applied as an effective vaccine platform for several human infections such as COVID-19, malaria, and Ebola [23–27]. To re-redirect the natural SAd36 vector tropism selectively to the vascular endothelium, we replaced the fiber knob region with the previously reported T4 fibritin-MBP sequence (SAd36. MBP) [9,10,28]. This targeting strategy resulted in a multi-vascular bed-targeting capacity. Particularly, endothelial cells (EC) of the kidney and brain have shown the highest transduction efficiency, whereas liver transduction drastically reduced compared to Ad5. Moreover, SAd36. MBP infection retained in vivo gene transfer even in the presence of neutralizing anti-Ad5 antibodies. Based on this feasibility, we next explored whether the SAd36. MBP could deliver Cre recombinase or CRISPR/Cas9 genome editor from Streptococcus pyogenes (SpyCas9) to the EC cells of these organs. In vivo analysis of the iv injected SAd36. MBP in the Ai9-SauSpyCas9 reporter mouse model revealed relevant tdTomato expression ECs of the spleen, brain, kidney, lungs and adrenal glands. Our study is the first to report in vivo editing of multi-organ endothelium by a systemically administered viral vector that evades the anti-Ad5 preexisting immunity. This platform provides a key technology feasibilizing gene editing-based gene therapy for the vascular endothelium.

2. Results

2.1. SAd36 vector with fiber incorporated MBP sequence exhibits a multi-vascular bed-targeting capacity

To assess the utility of the SAd36 as a gene transfer vector, we generated a replication-deficient vector by replacing the open reading frames of E1A and E1B with a transgene expressing a green fluorescent protein (GFP) reporter gene driven by the cytomegalovirus (CMV) promoter. For re-targeting purposes to the endothelial cells, we have employed a similar capsid modification that our group previously reported for human Ads [10]. In this regard, Lu et al. showed that the capsid-engineered human Ad5 with the fiber knob deleted and replaced by MBP ligand-T4 fibritin trimerization domain (Ad5. MBP) enables multiorgan vascular EC gene expression and reduced liver tropism [10]. We hypothesized that the SAd36 vector with the fiber knob replaced with MBP ligand-T4 fibritin (SAd36. MBP) recapitulates the multi-vascular bed-targeting capacity of the human Ad5. MBP vector (Fig. 1A). We compared the body-wide biodistribution of SAd36, SAd36. MBP versus Ad5 in mice following iv vector administration using immunofluorescence microscopy analysis. The study revealed that SAd36 lacks transduction in almost all organs examined (kidney, brain, heart, muscle, small and large bowel, pancreas) (Figs. 1B-C and S1), and exhibits reduced transduction of the liver compared to the human Ad5 adenoviral vector (Fig. 1D). The SAd36. MBP vector, however, showed strong GFP transgene expression in the spleen, kidney, and the brain (Fig. 1B-C). Co-staining of tissue sections with an endothelial cell (EC)-specific CD31/endomucin cocktail revealed that enhanced GFP expression was restricted to the vasculature in nonspleen organs. Of note, all the examined vectors showed transduction in the pulmonary vasculature. Furthermore, we quantified the fraction of vascular EC area expressing GFP in kidney and brain micrograph sections derived from SAd36. MBP-injected mice and compared to that from Ad5 and SAd36-injected mice (Fig. 1C). SAd36. MBP vector systemic injection results in a significantly higher transduction of kidney and brain endothelium compared to Ad5 or SAd36 viral vector injection (mean GFP^{+}/vascular area for brain and kidney 4.1% and 12.8%, respectively) (Fig. 1C). Moreover, GFP expression was observed almost exclusively in the vasculature of these organs (>50 and >90% of the GFP expression colocalized with the CD31/endomucin stained cells in the brain and kidney, respectively) and the GFP expression persisted from day 1 to day 15 post-injection (data not shown). Additionally, quantification of the GFP protein levels in tissue lysates revealed 80-fold reduction in the liver GFP level of SAd36. MBP injected mice compared to the liver GFP level of Ad5 injected mice (Fig. 1D).

In sum, these results suggest that the SAd36 vector, like Ad5, is suitable for capsid engineering, and incorporating an EC-specific MBP targeting ligand into the viral capsid alters vector tropism and retargets it to the endothelium of various organs. Furthermore, the drastically reduced liver transduction of SAd36. MBP makes this vector highly desirable for delivering therapeutic genes providing the means to circumvent potential hepatotoxicity associated with other viral vectors. In the present context, these technical feasibilities facilitated testing our main hypothesis regarding in vivo editing at the vascular endothelium.

2.2. SAd36.MBP retains an effective in vivo gene transfer in presence of pre-formed anti-Ad5 immunity

A key rationale to employ non-human Ads is their capacity to traverse pre-formed immunity to human Ad5 (hAd5). In this regard, a large portion of the population has pre-formed neutralizing antibodies (nAbs) against this major human serotype. To investigate whether SAd36. MBP could escape the host neutralization response against the hAd5 in vivo; we first injected C57BL/6 mice with phosphate-buffered saline (PBS or saline) or 10^{10} virus particles (VPs) of Ad5 per mouse via iv injection. Lower concentrations of iv injected Ad5 virus have been succeeded in

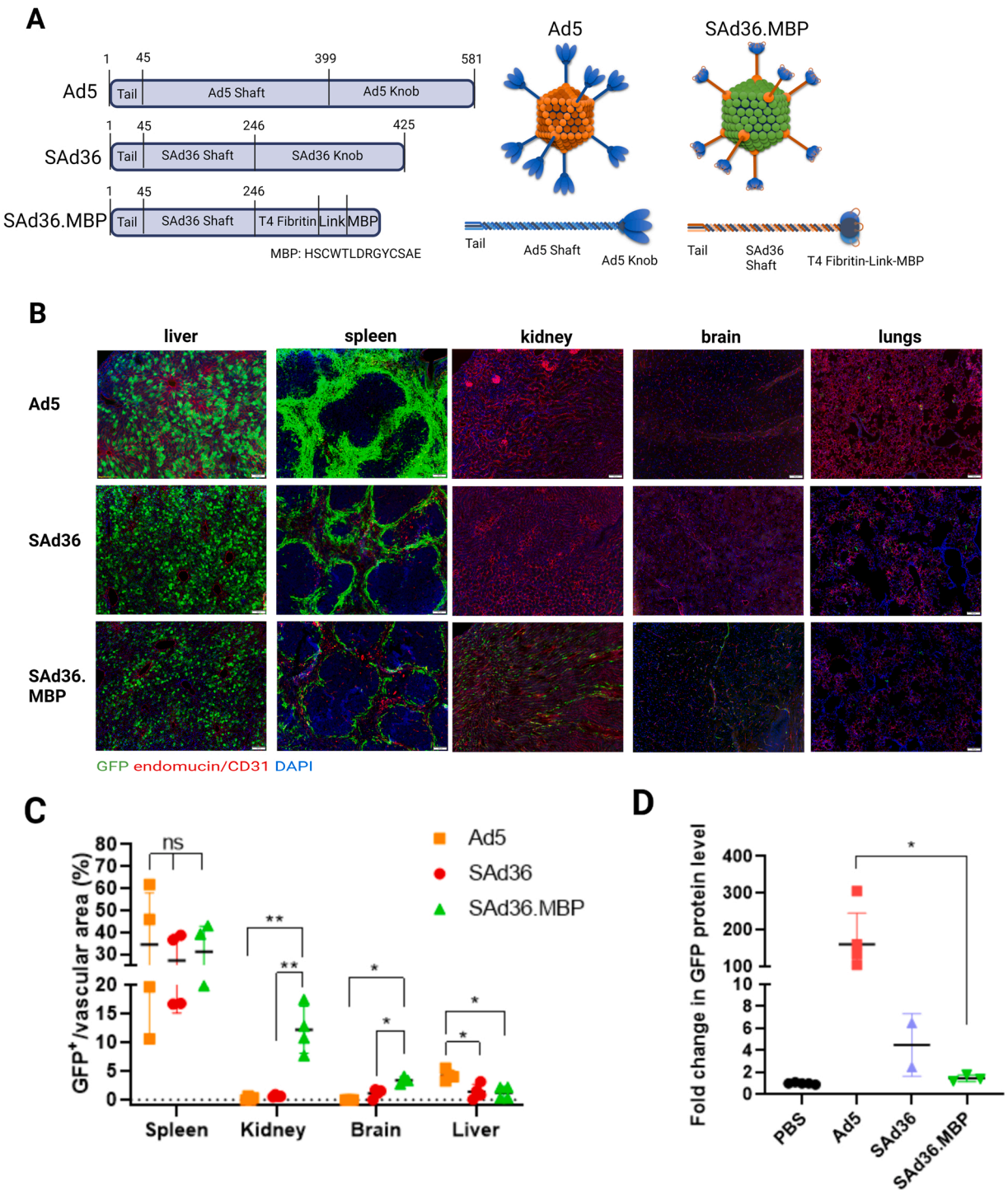

Fig. 1. SAd36 vector with fiber incorporated MBP sequence exhibits a multi-vascular bed-targeting capacity. (A) Schema to accomplish in vivo pan-endothelium targeting via the myeloid cell-binding (MBP) peptide incorporated into the simian adenovirus 36 (SAd36) capsid. To modify the vector tropism a strategy of fiber replacement was employed. Particularly, SAd36 fiber knob was deleted and replaced by the MBP ligand –T4 fibritin trimerization domain to get SAd36.MBP adenoviral vector. (B) Biodistribution of SAd36, SAd36.MBP, and Ad5 vector transgene expression in mice. Immunofluorescence microscopy analysis of vector GFP expression in host organs at day 3 following iv injection of 1.0 × 10^11 viral particles (vp) of Ad5 (n = 4), SAd36 (n = 4), and SAd36.MBP (n = 4) into C57BL/6 J mice. The study revealed that SAd36 lacks transduction in almost all organs examined (lungs, kidney, brain, heart, muscle, small and large bowel, pancreas) (see Fig. S1.) The SAd36.MBP vector, however, showed strong transgene expression in kidney and brain. (C) Costaining of tissue sections with an endothelial cell (EC)-specific CD31/endomucin cocktail revealed that enhanced GFP expression was restricted to the vasculature in nonspleen organs. The percentage of vascular EC area expressing GFP in each organ derived from Ad5.CMV-, SAd36.CMV-injected mice (n = 4 for all organs) versus that from SAd36.MBP.CMV-injected mice. Bar graph is mean + /- standard deviation, * $p < 0.05$, ** $p < 0.01$, *** $p < 0.001$, Magnifications, × 100. Red, CD31/endomucin; green, GFP; blue, DAPI. The GFP fluorescence exposure time was 120 ms for all organs. (D) C57BL/6 mice were injected with PBS or 10^{11} VPs of Ad5, SAd36, or SAd36.MBP.CMV.GFP per mouse by iv injection (n = 3–4 per group). Three days later, the mice were sacrificed and the livers were harvested for the GFP activity assay. The GFP protein level were normalized to the corresponding average GFP protein levels of PBS control mice. Bar graph is mean + /- standard deviation, * $p < 0.05$.

generating suitable nAbs to prevent reinfection of the Ad5 vector [29]. One month later, the mice were injected with PBS or 10^{11} VPs of Ad5, SAd36 or SAd36. MBP per mouse by iv injection (Fig. 2). Three days later, the mice were sacrificed, and their tissues were harvested for the GFP quantification assay. For this assay, the spleen was chosen as a target organ because all vector examined here exhibits a significant level of spleen transduction. As expected, the GFP protein levels of tissue lysates measured by the GFP quantification kit were significantly lower in the Ad5 pre-immunized mouse group than the group immunized by only PBS. This data confirms that Ad5 infection was blocked by Ad5 pre-immunization. On the other hand, SAd36. MBP infection was not blocked by anti-Ad5 neutralizing antibodies, as GFP protein levels of tissue lysates remained at a similar level in the Ad5-and PBS-preimmunized mice after SAd36. MBP iv injection (Fig. 2). Immunofluorescence microscopy analysis of GFP expression in the harvested tissues revealed the same pattern (data are not shown). Overall, our data indicate that Ad5 and SAd36. MBP (and SAd36) vectors were not cross-neutralized in vivo and SAd36. MBP (and SAd36) virus could overcome the host neutralization response to hAd5. This capacity potentially provides a key advantage vis-à-vis ultimate human clinical translation.

2.3. Successful production of CRISPR/Cas9 genome editor expressing SAd36.MBP vector

To generate SAd36. MBP vectors expressing CRISPR/Cas9 genome editors, we used an inducible system to suppress Cas9 expression in the Ad-producer 293 cell line. Previous studies noted difficulties during propagation or rescue of Cas9, transcription activator-like effector nuclease (TALEN), or zinc-finger nuclease (ZFN) endonuclease expressing Ad vectors [30,31]. To prevent the deletion of the CRISPR/Cas9 expression cassette or selection for recombinant vector genomes during virus production, we employed the tetracycline (Tet)-inducible transgene expression system [32]. The vectors were successfully rescued and propagated in TREx^{TM}-293 cell line expressing Ad5 wild type fiber (F5), created as described in Material and Methods.

We constructed Streptococcus pyogenes Cas9 (SpyCas9) containing SAd36. MBP vectors under the Tet-dependent CMV promoter (CMV. TetON); expressing the modified Ai9-SauSpyCas9 allele-specific guide RNA (gRNA) driven by U6 promoter either in forward or reverse orientation, SAd36. MBP.SpyCas9_FWD and SAd36. MBP.SpyCas9_REV, respectively (Fig. 3A). Orientation of the promoters of the two genome editing components, gRNA and Cas9, has been shown to affect gene-editing outcomes when delivered via AAV vector [33]. To investigate the effect of the orientation of the two transgenes expressed by Ad vector on gene editing efficiency, we transduced immortalized mouse embryonic fibroblast (MEF) cells derived from the Ai9-SauSpyCas9 reporter mouse line [34]. This reporter mouse model and its derivative MEF cell line express robust tdTomato fluorescence following the deletion of the loxP flanked stop cassette by single gRNA — SpyCas9 mediated non-homologous end joining (NHEJ) or Cre-mediated recombination. Six days post-transduction, transduced Ai9-SauSpyCas9 derived MEF cells were analyzed by fluorescence microscopy (Fig. 3B.) and flow cytometry (Fig. 3C). Gene editing efficiency was quantified based on tdTomato expression of the single-cell suspension prepared by trypsinization of the transduced MEF cells. There was no significant difference in the gene editing outcomes between SAd36. MBP.SpyCas9_FWD with the gRNA in the forward direction and the SAd36. MBP.SpyCas9_REV with the reverse-oriented guide based on dTomato expression measured by flow cytometry (Fig. 3C.). As expected, control vectors, the SAd36. MBP.Cre and the Ad5. Cre performed extensively better to induce tdTomato fluorescence signal due to the Cre-mediated recombination. Furthermore, the significant difference between the tdTomato expression of the Ad5. Cre and SAd36. MBP.Cre transduced cells could be explained by the higher transduction efficiency of MEF cells by the Ad5 backbone compared to SAd36. MBP. A similar tendency was observed between GFP expressing Ad5 and SAd36. MBP backbone vectors (data are not shown). Additionally, we validated the genome editing function of SAd36. MBP.SpyCas9 and SAd36. MBP.Cre vectors by next generation sequencing (NGS)-based deletion (Fig. S2.). The Cre recombinase expressing SAd36. MBP vector induced over 95% deletion at the Ai9-SauSpyCas9 locus, while transduction of the Ai9-SauSpyCas9 MEF cells by the SpyCas9 expressing vector resulted in only approximately 25% deletion. Based on our previous studies [3,4], we found the 25% deletion capacity of the SAd36. MBP.SpyCas9_FWD, SAd36. MBP.SpyCas9 hereafter, rational to move on to evaluate the functionality of these vectors in the Ai9-SauSpyCas9 mouse model in vivo.

2.4. SAd36.MBP adenoviral vector delivers CRISPR/Cas9 genome editor to the spleen, kidney, lungs, brain, and adrenal glands vasculature of the Ai9-SauSpyCas9 reporter mouse model

We assessed the capacity of the SAd36. MBP adenoviral vector to deliver CRISPR/Cas9 genome editor to the vasculature of Ai9-SauSpyCas9 reporter mouse model in vivo. The Ai9-SauSpyCas9 fluorescent reporter platform is originated from Ai9 mouse model, where the loxP-flanked stop cassette was modified so that a single gRNA for Streptococcus pyogenes or Staphylococcus aureus Cas9 (SpyCas9 and SauCas9, respectively) can guide Cas proteins to delete the stop cassette by NHEJ events which results in tdTomato activation [34].

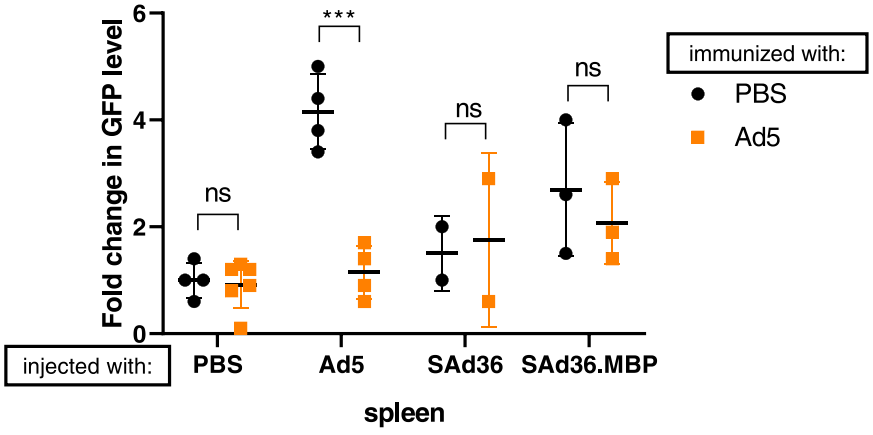

Fig. 2. Effective in vivo gene transfer in presence of preformed anti-Ad5 immunity. C57BL/6 mice were pre-immunized with PBS (saline) or 10^{10} VPs of Ad5.CMV. eGFP or SAd36.MBP.CMV.eGFP per mouse by intravenous (iv) injection (n = 15–15 per group). One month later, the mice were injected with PBS or 10^{11} VPs of Ad5, SAd36, or SAd36.MBP per mouse by iv injection (n = 3–4 per group). Three days later, the mice were sacrificed and the spleens were harvested for the GFP activity assay. The GFP protein level were normalized to the corresponding average GFP protein levels of PBS or Ad5-immunized PBS control mice. Ad5 infection was greatly inhibited by Ad5 pre-immunization. On the contrary, neither SAd36 nor SAd36.MBP infection was blocked, but retained to a same degree in the spleens of Ad5-preimmunized mice. Statistical analysis was performed using GraphPad PRISM software. Groups with normal distribution, determined by the Shapiro-Wilk test, were compared using parametric unpaired t-tests. All t-tests were two-tailed. For all statistical analyses p-values were denoted as > 0.05 (no significance [ns]), and < 0.001 (***). Scattered dot plot graph is mean + /- standard deviation.

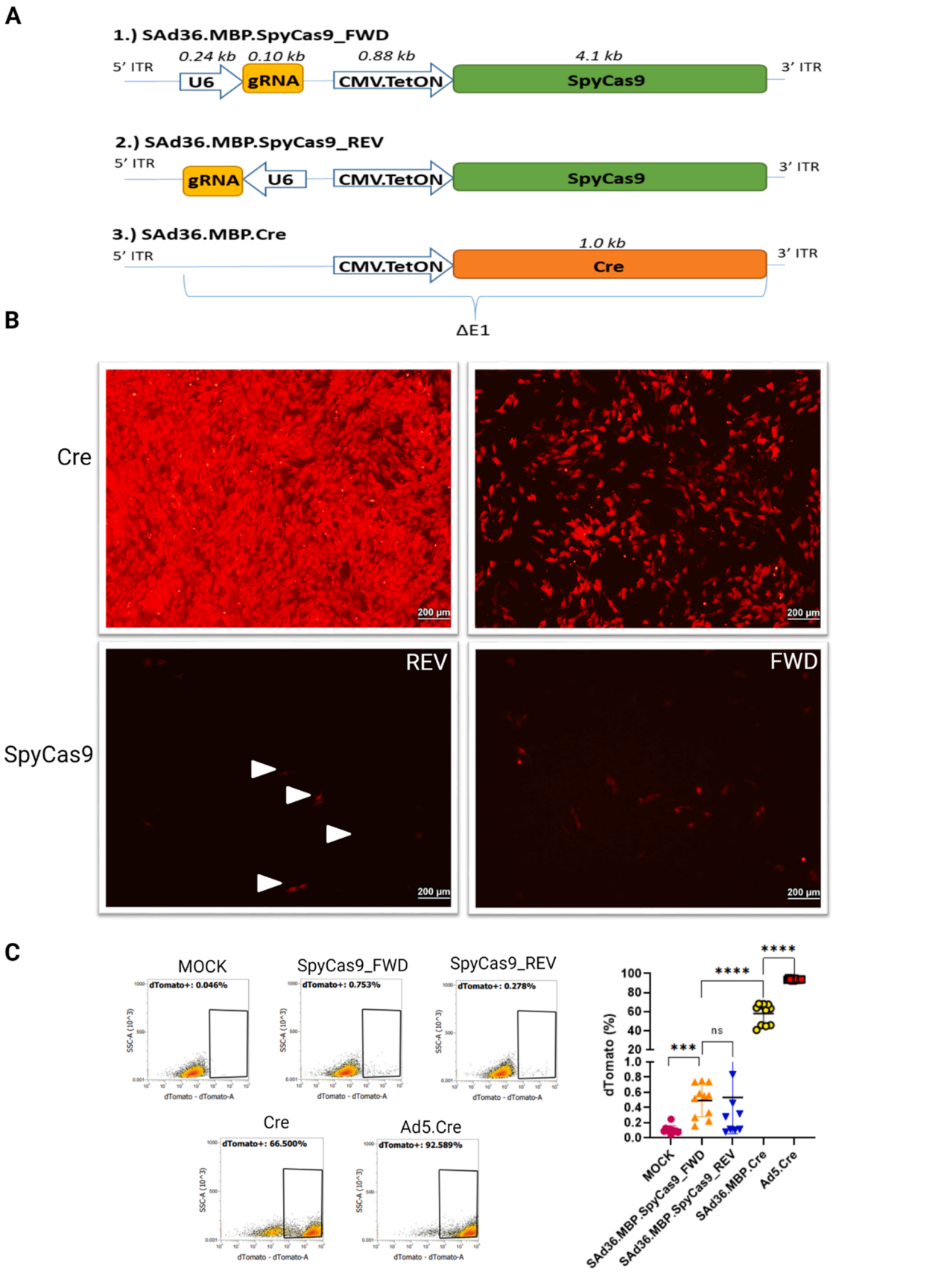

(caption on next page)

Fig. 3. In vitro validation of SpyCas9 expressing SAd36.MBP vectors. (A) A schematic of the adenoviral vectors used in this study. SAd36.MBP.SpyCas9_FWD (vector 1) expresses Streptococcus pyogenes Cas9 nuclease (SpyCas9) under control of the tetracycline-dependent CMV promoter (CMV.TetON) and the Ai9-SauSpyCas9 allele-specific guide RNA (gRNA) driven by U6 promoter in forward orientation to induce double-stranded breaks at the target site. SAd36.MBP.SpyCas9_REV (vector 2) expresses CMV.TetON driven SpyCas9 and U6 driven gRNA in reverse orientation to evaluate whether orientation of the two transgenes affect gene editing efficiency. Control vector (SAd36.MBP.Cre, vector 3) consists of Cre recombinase under the CMV.TetON promoter. All SAd36.MBP vectors were transfected and propagated in TREx^{TM}-293 cell line expressing Ad5 wild type fiber (F5) (TREx^{TM}-F5 cell line). (B) Immortalized mouse embryonic fibroblast (MEF) cells (5×10^4 cells) derived from Ai9-SauSpyCas9 mice were infected with Ad5.Cre (top left), SAd36.MBP.Cre (top right), SAd36.MBP.SpyCas9_REV (bottom left) and SAd36.MBP.SpyCas9_FWD (bottom right) at a multiplicity of infection (MOI) of 5000, and tdTomato expression (red) were imaged on six days post virus infection (6 dpi) using fluorescence microscopy and (C) flow cytometry. Magnifications, × 100; Red, tdTomato; fluorescence exposure time for tdTomato, 333 msec. **(C)** Quantification of in vitro gene editing efficiency based on the percentage of tdTomato$^+$ MEF cells by flow cytometry analysis at 6 dpi.

We administered 6×10^{10} VPs or 1×10^{11} VPs of the SAd36. MBP. SpyCas9 vector (4 mice per group), 6×10^{10} VPs of the SAd36. MBP.Cre vector as positive control (2 mice), and saline solution as negative control (4 mice) via tail vein injection. Seven days post-injection whole-body biodistribution study by immunohistochemistry (IHC) was conducted to assess tdTomato expression in the vasculature of different organs (spleen, liver, lungs, kidney, adrenal glands, brain, heart, colon, diaphragm, duodenum, epididymis, eye, gastrocnemius, ileum, jejunum, ovary, pancreas, white and brown adipose tissues, soleus, stomach, testes and uterus) (Figs. 4 and S3).

Among all organs examined, spleen, liver, lungs, and adrenal glands showed relevant tdTomato signal in both the SAd36. MBP.SpyCas9 and SAd36. MBP.Cre injected Ai9-SauSpyCas9 mice, and these signals correlated well with the lectin-labeled endothelium (Figs. 4 and S3). Interestingly, brain (thalamus) had tdTomato signal in mice injected with SAd36. MBP.Cre, but no tdTomato signal was detected in the SpyCas9 expressing vector injected mice. Particularly high level of co-localization of tdTomato+ and lectin signals was observed in the spleen (54.3%), brain thalamus (6.6%) and lungs (2.2%) of the SAd36. MBP.Cre injected animals (Figs. S3 and S4). The results revealed by IHC co-localization analysis confirm that the SAd36. MBP adenoviral vector specifically targets and edits endothelial cells in the Ai9-SauSpyCas9

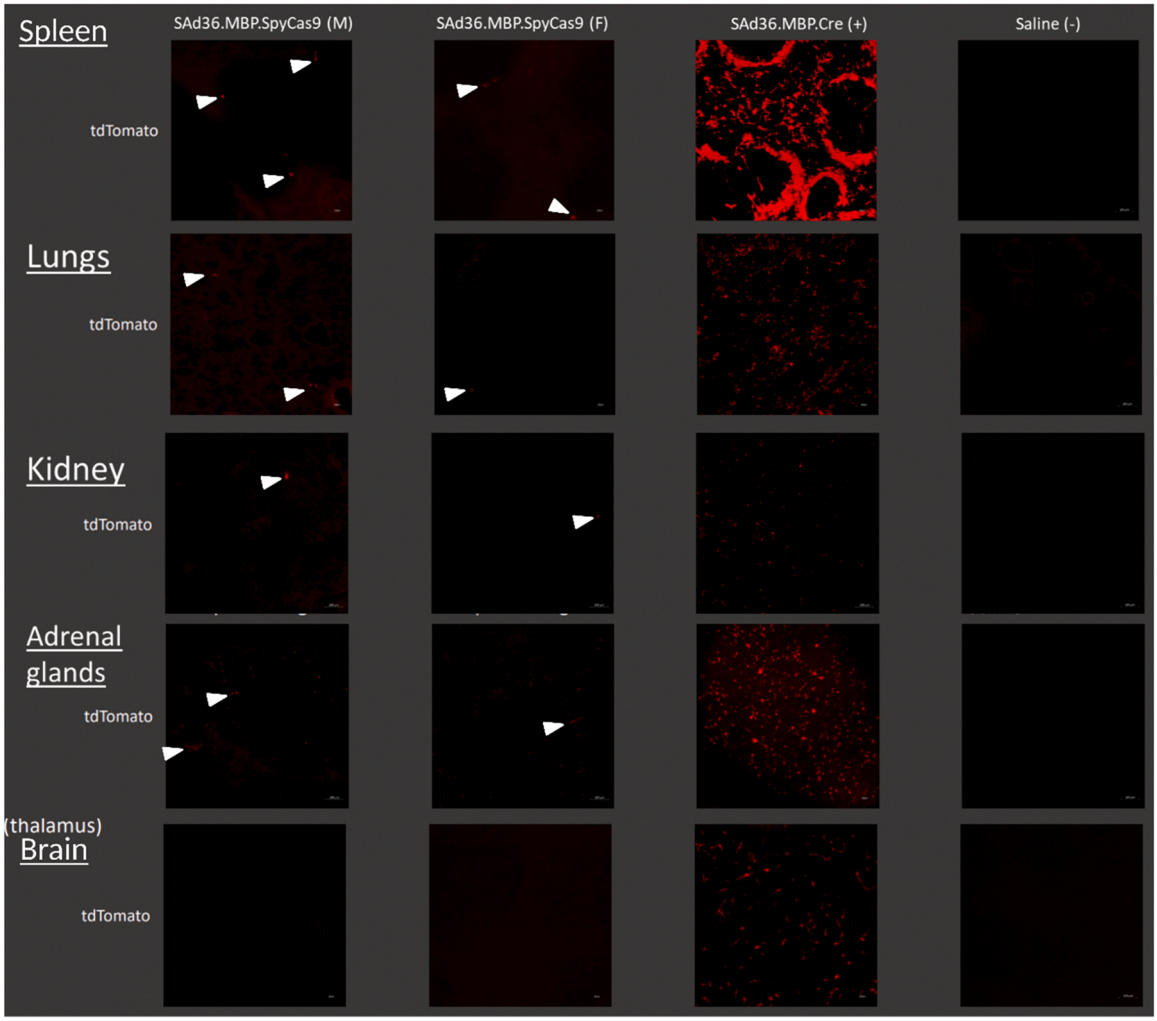

Fig. 4. External in vivo validation of SpyCas9 expressing SAd36.MBP vector in the Ai9-SauSpyCas9 mouse. 6–10 weeks old Ai9-SauSpyCas9 reporter mice were injected with either 6×10^{10} (two female (F) and two male (M)) or 1×10^{11} (two F and two M) virus particles (VPs) of SAd36.MBP.SpyCas9 adenoviral vectors in 160 µl of saline via the tail vein. As positive control (+), two mice (one F and one M) were injected with 6×10^{10} VPs SAd36.MBP.Cre, and as negative control (-), four mice (two F and two M) were injected with 160 µl saline solution. Tissues were harvested 7 days post administration. The frozen tissue sections were imaged on a Zeiss Axio Scan.Z1 scanner, using the 20X objective and Cy3 (for tdTomato, red signal) fluorescence filter. The external validation study was performed by researchers at Baylor College of Medicine and Rice University (BCM-Rice) in the frame of Somatic Cell Genome Editing (SCGE) Consortium.

mouse.

For quantification of the tdTomato+ cells in cell population expressing CD31 and CD102 endothelial cell specific biomarkers, we thought to conduct flow cytometry analysis in the organs (spleen, lungs, adrenal glands) that showed the highest-level tdTomato expression in the whole-body biodistribution study. The adapted protocol from Wang et al. and Dumas et al. was not suitable for isolation of brain endothelial cells [35,36]. Ai9-SauSpyCas9 mice were iv injected with 1×10^{11} VPs of either the SAd36. MBP.Cre vector or SAd36. MBP.SpyCas9 or with saline (7–10 mice per group). Seven days later, we harvested spleens, lungs and adrenal glands and prepared single cell suspensions subjected for flow cytometry analysis.

SAd36. MBP.Cre vector induced significantly higher tdTomato signal in both $CD31^+$, $CD102^+$ cell populations compared to the saline injected group (Mean tdTomato signals in $CD31^+$ EC cells of the lungs, adrenal glands and the spleen, respectively: 3.85, 0.80, 0.71%; mean tdTomato signals in $CD102^+$ EC cells of the lungs, adrenal glands and the spleen, respectively: 3.81; 0.92; 0.56%). However, we could not observe significant level of tdTomato signals in the $CD31^+$ or $CD102^+$ EC cells of these organs in the SAd36. MBP.SpyCas9 group analyzed by flow cytometry (Fig. 5).

3. Discussion

In the present study, we report a vascular endothelium-targeted nonhuman adenoviral vector, SAd36. MBP, which can evade the pre-existing human adenovirus serotype 5 (hAd5) immunity and induce genome editing selectively in the vascular endothelium through the delivery of Cre recombinase or CRISPR/Cas9 nuclease.

Numerous strategies could circumvent pre-existing immunity against hAd5 such as a prime-boost regimen, alternating immunization routes and nonhuman adenovirus serotypes [22]. Animal-derived adenoviruses such as simian, bovine, and ovine have been developed since nAbs against these viruses are rare in human populations. Nevertheless, besides humoral ones, cellular immune responses must be considered since cross-reactive Ad specific T-cells could decrease adenoviral vector efficacy [22]. On this note, the simian adenovirus species E serotype 35 (SAd36) has previously shown low seroprevalence in human populations and emerged as a safe vaccine platform in preclinical studies and is currently being validated in clinical trials [24–26].

In addition to its utility as a genetic vaccine, SAd36 with a pan-endothelium-targeting ligand myeloid cell-binding peptide (MBP) incorporated in the capsid has allowed targeted delivery to the vascular endothelium. Targeting endothelial monolayer of selective organs could lead to the development of potential novel therapeutics for both benign and malignant diseases characterized by endothelial dysfunction such as atherosclerosis, Alzheimer's, glioblastoma, sepsis, acute respiratory distress syndrome, and COVID-19 respiratory distress and cardiovascular diseases [37–43]. Additionally, EC-targeted adenovirus that mitigate liver toxicity could provide an effective means to transduce organ-specific vascular endothelial subsets, providing an important source of therapeutic serum factors for the treatment of systemic diseases. We observed low liver gene transfer efficiency of SAd36. MBP; however further studies are required to evaluate if this correlates with reduced liver inflammatory damage compared with that caused by hAd5.

We showed that after seven days of a single iv administration of Cre recombinase expressing SAd36. MBP results in precise genome editing events and consequently activation of the tdTomato gene in the spleen, brain thalamus, lungs, and adrenal glands of the Ai9-SauSpyCas9 reporter mouse model. In vivo vascular fluorescence labeling by lectin dye confirmed that large number of the tdTomato+ cells in these organs are

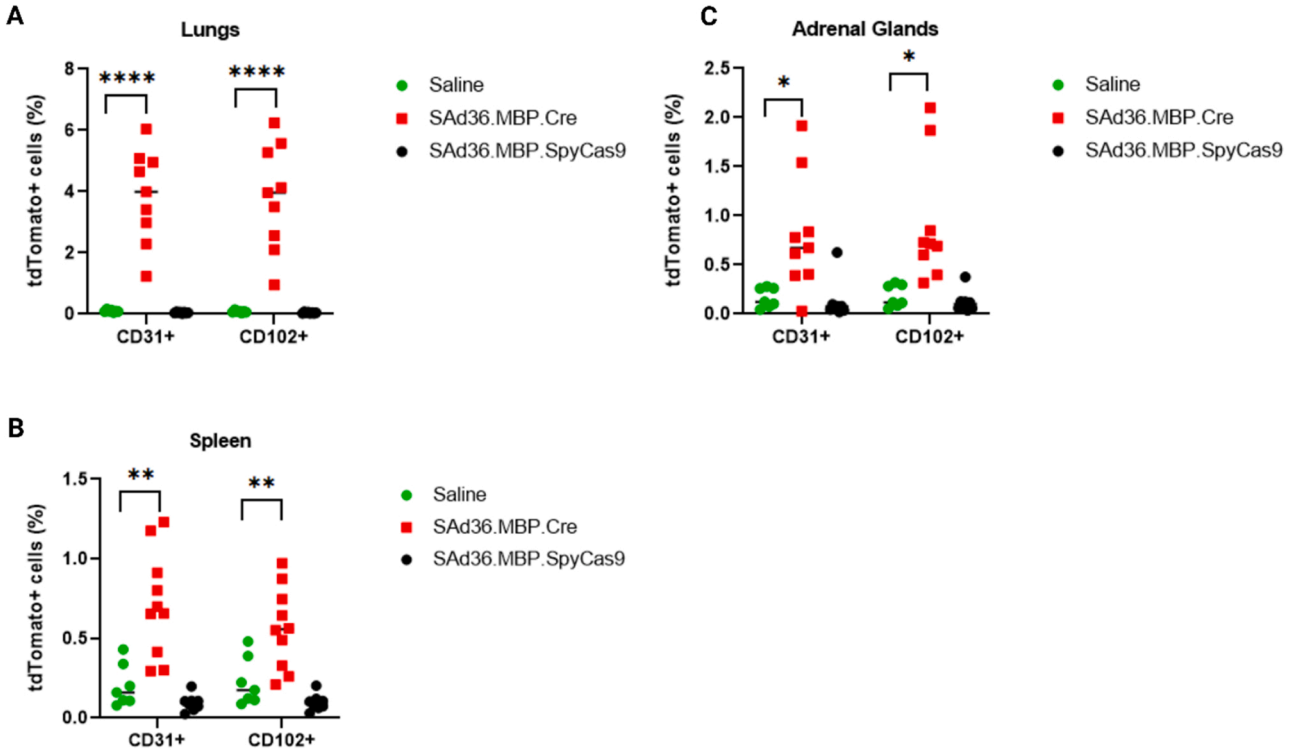

Fig. 5. Quantification of tdTomato$^+$ signal by flow cytometry analysis in the $CD31^+$, $CD102^+$ endothelial cells of multiple mouse organs. 6–10 weeks old Ai9-SauSpyCas9 reporter mice were iv injected either with 1×10^{11} VPs of the SAd36.MBP.Cre vector, SAd36.MBP.SpyCas9 or 160 µl saline (7–10 mice per group). Seven days later, lungs, spleen and adrenal glands were harvested, and the single cell suspensions were subjected for flow cytometry analysis by Attune NxT flow cytometer using YL-1 laser (ThermoFisher). Data from three replicate experiments were combined in each graphs. Mean tdTomato signals in $CD31^+$ EC cells of the lungs, adrenal glands and the spleen, respectively: 3.85, 0.80, 0.71%. Mean tdTomato signals in $CD102^+$ EC cells of the lungs, adrenal glands and the spleen, respectively: 3.81; 0.92; 0.56%.

endothelial cells. Additionally, the more quantitative and sensitive flow cytometry analysis of SAd36. MBP.Cre injected animals have revealed close to 4% and 1% tdTomato expression in $CD31^+$ and $CD102^+$ endothelial cell populations in the lung and spleen, respectively.

Recent studies have achieved efficient genome editing in mouse liver with either viral [3,4,44] or non-viral vector [45,46] delivery of genome editors; however, effective and selective editing of specific cell types with a single therapeutic agent and without unwarranted nontarget cell genome modification remains challenging. We acknowledge the remarkable development of nanoparticle delivery of CRISPR/Cas plasmid DNA that induced highly efficient genome editing, 37% indel rate, in vascular EC cells of multiple organs (heart, lung, aorta) with about 20% indels in hepatocytes [8]. Nevertheless, we believe that targeted adenoviral vectors will earn their place in the toolbox for promoting genome-editing applications. Targeted nonhuman adenoviral vectors combined with CRISPR/Cas knock-in technology could traverse field barriers, including protective local protein production, long-term gene correction with minimized off-target effects, mitigated liver toxicity, and circumvented preformed immunity. Moreover, using vascular endothelium as a non-hepatic cellular source might embody an excellent gene-therapy solution for several inherited genetic diseases such as alpha-1 anti-trypsin deficiency [3,5,47], hemophilia A and B [4], mucopolysaccharidoses type I [2].

While our data fully validate specific cargo delivery and gene editing in the targeted endothelial cells by the modified SAd36 adenoviral vector, further studies are required to optimize the efficacy of the CRISPR/Cas9 nuclease mediated cleavage. The failure to observe higher gene editing activity in the SAd36. MBP.SpyCas9 injected animals might be due to insufficient expression of the Cas9 nuclease by the CMV.TetON promoter, insufficient gRNA expression by the U6 promoter, or both. Nevertheless, Western blot analysis for Cas9 suggests that Cas9 was expressed at a detectable level in kidney and liver (Fig. S5.). Since we administered the highest adenoviral vector dose that does not induce tissue toxicity in mice, in future studies stronger or endothelial cell-specific promoters, such as CAG and CDH5, could be employed to drive higher Cas9 expression in the vascular endothelium [8,48]. Additionally, choosing an alternative gRNA target sequence or an alternative route to express both Cas9 and gRNA might be the solution for achieving higher gene editing efficiency. To this end, we recently developed an adenoviral "piggyback" approach to deliver CRISPR/Cas9 components as ribonucleoprotein (RNP) enzyme complexes on the surface capsid proteins of the SAd36 vector [49]. The gene editing efficiency of this Plug-and-Play platform was comparable with commercial CRISPR/Cas9 transfection reagent when applied on Ai9-SauSpyCas9 derived MEF cells and much higher compared to the DNA expression vector CRISPR/Cas9 delivery method of SAd36. MBP [49]. Nevertheless, a direct comparison of the two systems is warranted in the future.

We anticipate combining an endothelium-targeted nonhuman adenoviral vector that provides a shield against neutralizing antibodies, such as the above-described SAd36. MBP, with the smart "piggyback" technology, will result in a versatile tool for safe, specific and effective genome editing applications and beyond.

4. Conclusions

To our best knowledge, the SAd36. MBP vector is the first targeted adenoviral vector showing in vivo genome editing activity in endothelial cells of multiple organs in a reporter mouse model. Moreover, we have shown that SAd36. MBP vector is capable of delivering transgenes in the potential presence of pre-formed anti-Ad vector immunity. Furthermore, it has a significantly reduced capacity to target the liver hepatocytes compared to the hAd5. This study serves as a proof-of-principle for the in vivo adenoviral delivery of genome editing machinery into disease-relevant cells and tissues. More studies are required to increase the genome editing activity of the CRISPR/Cas expressing SAd36. MBP vector; however, we demonstrated the excellent prospect of targeted adenoviral delivery systems for future clinical gene editing.

5. Material and methods

5.1. Adenoviral vector constructions

The replication incompetent Ad5. CMV.eGFP vector was constructed using the E1-deleted Ad5 backbone as we previously described [50,51]. We employed pC36.000.cmv.PI.EGFP.BGH plasmid carrying the genome of chimpanzee species E adenovirus SAd36, in which the early E1 region was replaced by a CMV promoter-hybrid intron-eGFP cassette [52]. We further engineered E3 region-deleted pC36.000.cmv.PI.EGFP. BGH viral genome by removing a 4384 bp fragment from a unique *Bsp*EI site to the E3 14.7 K stop codon, which includes seven genes: E3 CR1-a, E3 gp19K, E3 CR1-b, E3CR1-g, E3 RID a, E3 RID b, and E3 14.7k[25]. To engineer SAd36 fiber modification, we created a pSAd36 fiber shuttle vector, in which a 7352 bp *Swa*I/I-CeuI fragment released from the viral genome was recirculated with a stuff DNA and Gibson ends flanked by *Sac*II and *Stu*I sites. A 1076 bp *Mfe*I/*Pvu*II fragment from the shuttle plasmid was replaced by a 1003 bp synthesized fiber-T4 fibritin-MBP (ffMBP) fragment via Gibson assembly. Specifically, the fiber knob region (sequences encoding codon 246 to the last codon 425) was replaced by 285 bp bacteriophage T4 fibritin domain, 45 bp sequence encoding a flexible linker, and sequences encoding MBP to derive pSAd36.ffMBP shuttle. To generate pSAd36. E3D.ffMBP, the fragment containing the modified fiber was released with *Sac*II and *Stu*I and ligated back to a 30, 789 bp I-CeuI/*Swa*I viral genome fragment via Gibson assembly. To generate the CMV.TetON promoter driven SpyCas9 or Cre and the U6 promoter driven gRNA expressing pSAd36. E3D.ffMBP vectors, we applied the strategy originally reported by Roy et al. [52]. First, the SpyCas9-coding and U6-driven loxP gRNA target sequences were PCR-amplified with primers SpyCas9_fwd (CGTACGGTCCAACTG-CAGCCGGGACTATAAGGACCACGACG), SpyCas9_rev (GGCCCTCC TCCCCAGCATGCCTG), and loxPgRNA_fwd (CTGGGGAGGAGGGCCCG-TACGTATTTCCCATG), loxPgRNA_rev (TTTTCACCTAAATTTCCGCG-TACGCAAAAAAGCACCGACTCGG) from CRISPRmTmG2. The plasmid was a kind gift from Connie Cepko (Addgene plasmid # 69992; http://n2t.net/addgene:69992; RRID: Addgene_69992) [53]. The CMV. TetOn promoter expressing pSAd36-E1-shuttle plasmid was digested with *Bsi*WI and *Acc*65I restriction enzymes, followed by NEBuilder® HiFi DNA Assembley Reaction (NEB #E2621) with the two PCR fragments mentioned above. The resultant pSAd36-E1-shuttle.CMVTetON. SpyCas9. U6.gRNA(loxP) plasmid was digested with *Bsi*WI restriction enzyme to enable NEBuilder® HiFi DNA Assembley with the DNA fragment encoding the Ai9-SauSpyCas9 allele targeting gRNA sequence (Sequence 5' to 3' (PAM): GTATGCTATACGAAGTTATT (AGG)) under the U6 promoter [54]. The resultant plasmid, pSAd36-E1-shuttle. CMVTetON.SpyCas9. U6.gRNA(Ai9)_REV was digested with PspOMI/*Stu*I to flip the CMVTetON.SpyCas9 fragment in the forward orientation with U6.gRNA. The resultant plasmid was named pSAd36-E1-shuttle.CMVTetON.SpyCas9. U6.gRNA(Ai9)_FWD. The *Pme*I-linearized pSAd36-E1-shuttle plasmids were recombined with the viral pSAd36. E3D.ffMBP genome in *Escherichia coli* strain BJ5183 as described elsewhere[55]. The constructed viral genomes SAd36. MBP. SpyCas9_FWD, SAd36. MBP.SpyCas9_REV and SAd36. MBP.Cre were released from plasmid DNA by digestion with *Pac*I and transfected into TREx^{TM}-F5 cell line. TREx^{TM}-F5 cell line was derived from TREx^{TM}-293 cell line (Invitrogen), and constitutively expresses the wild-type Ad5 fiber protein (F5) to be incorporated into the viral capsids, similarly to 293F28 cell line that was generated and employed in-house[56,57]. The rescued replication-incompetent SAd36. MBP vectors were upscaled in TREx^{TM}-F5 cell line and then were purified using cesium chloride density gradient ultracentrifugation following the final passage in 293 cells in order to produce viral progeny containing only the chimeric fiber-fibritin-MBP. Purified virus preparations were dialyzed against 10% glycerol in phosphate-buffered saline (PBS), and the number of

virus particles (vp) was determined based on absorbance at 260 nm as described by Mittereder et al.[58], and were as follows: for SAd36. MBP. SpyCas9_FWD, 1.8×10^{12} vp/ml; for SAd36. MBP.SpyCas9_REV, 2.7×10^{11} vp/ml; and for SAd36. MBP.Cre, 7.5×10^{11} vp/ml.

5.2. In vitro transduction and flow cytometry analysis

The immortalized mouse embryonic fibroblast (MEF) cell line derived from Ai9-SauSpyCas9 mouse model (MMRRC strain #068227-JAX) was seeded at 5×10^4 cells per well on twelve well plates after 1–2 h virus transduction at a multiplicity of infection (MOI) of 5000 with SAd36. MBP.SpyCas9_FWD, SAd36. MBP.SpyCas9_REV, SAd36. MBP.Cre and Ad5. Cre viruses. Six days later, tdTomato$^+$ cells were imaged with fluorescence microscopy. Next, cells were harvested by trypsinization (0.25% Trypsin- 0.1% EDTA, Corning^{TM}) either for deletion test at the Ai9-SauSpyCas9 locus (Fig. S2) or flow cytometry analysis (Fig. 3C). Deletion tests were performed by WashU Genome Engineering and iPCS Center (GEiC). Shortly, JK287. DS.F1 (tctgctaac-catgttcatgcc) and JK287. DS.R2 (caccttgaagcgcatgaact) primers were used to amplify the Ai9-SaiSpyCas9 allele region outside of the target sides. If deletion is present because of SpyCas9-induced NHEJ event or Cre-recombination, smaller than the predicated wild type amplicon (<891 bp) can be detected on the agarose gel. The Quantification of the tdTomato$^+$ cell population was determined by flow cytometry analysis using Attune^{TM} NxT Flow Cytometer using YL-1 laser (ThermoFisher). The results are from three independent experiments.

5.3. Animal studies

The Animal Studies Committee of Washington University in St. Louis approved all experimental procedures. Mice of the C57BL/6 J mouse background were obtained from The Jackson Laboratory (Bar Harbor, ME, USA), and mice of 6–10 weeks of age were used for experiments. The Ai9-SauSpyCas9 reporter mouse line (MMRRC stock #68227) and its derivative MEF cell line were obtained from BCM-Rice Small Animal Testing Center as part of the Somatic Cell Genome Engineering (SCGE) Consortium [34].

5.4. Virus injection and organ harvest for in vivo biodistribution studies in C57BL/6 mice

Mice were injected with 6×10^{10} or 1×10^{11} virus particles of SAd36. MBP adenoviral vectors in 160 μl of saline via the tail vein. At three or seven days post-vector injection, mice are induced into deep anesthesia with 2.5% 2,2,2-tribromoethanol (Avertin; Sigma-Aldrich, St. Louis, MO), and the thorax is opened. A 24-gauge round ball-tipped stainless oral gavage needle is inserted into the left ventricle, and the mouse was perfused with 30 ml of 10% PBS-buffered formalin or 4% paraformaldehyde (PFA). Organs are removed and undergo post-perfusion fixation in formalin at room temperature for 1–2 h or in 4% at 4 °C overnight. The fixative is washed out by three times 20 min ice cold PBS, followed by step wise increase to 30% sucrose in PBS (10%, 20%, 30%) at 4 °C until tissue sinks in each solution. Next, organs are embedded in NEG-50 mounting medium (Thermo Fisher Scientific, Waltham, MA), and frozen on dry ice. Once frozen, stored at − 80 °C.

5.5. In vivo neutralization

C57BL/6 mice were pre-immunized with PBS or 10^{10} VPs of Ad5. CMV.eGFP or SAd36. MBP.CMV.eGFP per mouse by iv injection. Each group contained nine mice. One month later, the mice were subjected to a second iv injection with PBS or 1011 VPs of Ad5 or SAd36. MBP per mouse (3–3 mice per group). Three days later, the mice were sacrificed, and their livers and spleens were harvested and frozen in liquid Nitrogen. The organs were homogenized on dry ice, lysed in Assay buffer (Cell Biolabs, AKR-120), and centrifuged at 5000 rpm at 4 °C. The supernatant was stored at − 80°C until GFP quantification described below.

5.6. GFP quantification from organ lysates

GFP protein levels in the harvested tissues were quantified according to the manufacturer's instructions (Cell Biolabs, AKR-120). Shortly, supernatants (100 μl) from homogenized tissue lysates were transferred to a 96-well plate suitable for fluorescence measurement. A dilution series of recombinant GFP standards (0–10,000 ng/ml) were prepared. Each sample, blank, and standards were assayed in triplicate, and fluorescence was measured with Bio-Tek Synergy HT Microplate Reader at 488 nm/507 nm.

5.7. Immunofluorescence staining

For immunofluorescence, frozen tissues are sectioned at 12 μm in thickness. Frozen-section slides are dried at room temperature for 10 min, washed three times in PBS to remove the NEG-50 mounting medium, and incubated with a protein block solution (5% donkey serum and 0.1% Triton X-100 in PBS) at room temperature for 1 h and then at 4 °C in protein block containing primary antibodies overnight. The primary antibodies for endothelial cell detection (CD31/endomucin cocktail): rat anti-endomucin (1:200, catalog number: 14–5851–81, eBioscience) and armenian hamster anti-CD31 (1:200, catalog number: MAB1398Z, MilliporeSigma). For tdTomato detection, we use goat anti-tdTomato primary antibody (1:100, SICGEN, ab8181–200). The detect SpyCas9, we used mouse anti-SpyCas9 primary antibody (1:400, 14697, Cell Signaling Technology). On day 2, the slides are washed three times in PBS, incubated with corresponding 1:400-diluted Alexa Fluor 488 (anti-rat and anti-armerian hamster)- and Alexa Fluor 594-conjugated secondary antibodies (anti-goat and anti-mouse) (Jackson ImmunoResearch Laboratories, West Grove, PA), and counterstained with SlowFade Gold antifade mounting reagent with 4′,6-diamidino-2-phenylindole (DAPI; Thermo Fisher Scientific). Immumofluorescence micrographs were acquired using an Olympus BX61 microscope equipped with a DP80 dual-sensor monochrome and color camera (Olympus America, Center Valley, PA).

5.8. Immunofluorescence microscopy-based analysis of viral reporter gene expression

CellSens Dimension imaging software (Olympus Soft Imaging Solutions) were applied to analyze colocalization of viral reporter GFP (green) and CD31/endomucin (vascular endothelium, red) gene expression. The optimized camera acquisition time for green and red immunofluorescence channel is set a priori for each organ within individual experiments and between experiments. The images, taken with 10x objective, are analyzed with Olympus CellSens Dimension Software using "Colocalization" and "Count and Measure" layout. A threshold defining the background signal intensity was set using non-virus-injected control tissues. A region of interest (ROI) was drawn over the tissue area based on suitable vascular EC staining within each micrograph. To identify fluorescence intensities where the individual fluorescences (red and green) overlap, "Colocalization" layout was applied. To evaluate the fraction of the vascular EC area expressing GFP, the endothelial marker-positive area and the reporter-positive area within the tissue ROI were quantified using "Count and Measure" layout. The GFP-positive area (GFP$^+$) was calculated as a percentage of the EC-positive area in the micrograph. Micrographs were taken in 4 biological replicates for each organs (spleen, kidney, brain, liver).

5.9. External validation of SAd36.MBP vectors by Baylor/Rice Small Animal Testing Center in Ai9-SauSpyCas9 reporter mouse

6–10 weeks old Ai9-SauSpyCas9 reporter mice were injected with

either 6×10^{10} (two female and two male) or 1×10^{11} (two female and two male) virus particles (VPs) of SAd36. MBP.SpyCas9_FWD adenoviral vectors in 160 µl of saline via the tail vein. As positive control, two mice (one female and one male) were injected with 6×10^{10} VPs SAd36. MBP.Cre, and as negative control, four mice (two female and two male) were injected with 160 µl saline solution. After 7 days post administration, all mice were given 100 µl bolus of lectin solution at 1 mg/ml (Vector Labs, DL-1178–1) via retro-orbital injection to label the vascular endothelial cells [59]. Following euthanasia via CO_2, two additional doses of lectin solution were given via transcardiac perfusion (100 µl to the left ventricle followed by 50 µl to the right ventricle) with a waiting period of one minute after each injection to allow the lectin to circulate. Following lectin staining, blood were flushed via transcardiac perfusion with saline solution, followed by perfusion with 4% paraformaldehyde (PFA) to initiate fixation. Afterwards, organ were harvested. The liver, lungs, and brain were fixed by immersion in PFA (drop fixation). Fixation were performed in a ratio of at least 20:1 (volume fixative to volume tissue) in 4% PFA, at 4 °C overnight, with gentle rotation to ensure adequate fixation. After overnight fixation, the samples were transferred to 30% sucrose solution (in saline) at 4 °C and incubated overnight. After equilibration in 30% sucrose/saline, the tissues were embedded in a trapezoidal Peel-A-Way embedding mold, and immersed in Optimal Cutting Temperature (OCT) compound and let to equilibrate for 30 min at room temperature (RT). Then, the tissues were mount in OCT by freezing the mold on dry ice. Once frozen, the molds were processed immediately or stored at − 80 °C for no longer than 1 month. For most organs 20-micron sections, and for brain 40-micron coronal sections were collected. For each tissue, sections were collected across multiple slides serially. Three non-consecutive sections on a single slide were subjected to imaging tdTomato signal to assess Cre-recombined or edited cells, DAPI to label nuclei, and lectin to visualize endothelial cells. For each tissue, one slide was mounted with DAPI stain. The frozen tissue section were imaged on a Zeiss Axio Scan.Z1 scanner, using the 20X objective and Cy3 (for tdTomato) and DAPI, Far-red Cy5 (for lectin) fluorescent filters. The co-localization analysis was performed using the Zen Blue software from Zeiss.

5.10. Quantification of tdTomato signals in the endothelial cells of mouse tissues by flow cytometry analysis

Mouse tissue dissociation and digestion procedures for endothelial cell analysis were adapted from Wang et al. [35] Shortly, mouse lungs, spleen, kidney and adrenal glands were harvested, cut into small pieces and shredded using scissors about 100 times followed by incubation with 3 mg/ml collagenase I (Life Technologies) for 45 min with shaking. After digestion, the tissue suspension was passed through 5 ml syringe with 20 G cannula attached, and triturated clumps into a single cell suspension, at least 12 times. The minced tissue was filtered through a 70-µm cell strainer (Miltenyi Biotec) and blocked with FBS containing media. After centrifugation, cell pellets were re-suspended in 0.5% BSA (bovine serum albumin), 2 mM EDTA containing PBS solution (PEB buffer) and applied to 30- µm pre-separation filter. Following centrifugation, cell counting, blocking with mouse FcR Blocking Reagent (Miltenyi Biotec) to avoid Fc receptor-mediated antibody labeling, the cells were stained for 30 min at 4 °C with PE Cyanine 7 conjugated CD31/PECAM-1 and Alexa Fluor 488 conjugated CD102/ICAM-2 antibodies (eBioScience) and subjected for flow cytometry analysis by Attune NxT flow cytometer (ThermoFisher) to quantify $tdTomato^+$ signal in $CD31^+$ or $CD102^+$ endothelial cell populations.

5.11. Statistics

All statistical analysis was performed using GraphPad PRISM software. Groups with normal distribution, determined by the Shapiro-Wilk test, were compared using parametric unpaired t-tests. If the groups had significantly different variance, determined by F-test, we used an unpaired t-test with Welch's correction for the groups' comparison. All t-tests were two-tailed. For all statistical analyses p-values were denoted as > 0.05 (no significance [ns]), < 0.05 (*), < 0.01 (**), or < 0.001 (***)).

Funding

This work was funded by NIH grants UG3 TR002851 awarded to D.T. C. This work was initiated and completed as part of our involvement in the NIH Somatic Cell Genome Editing (SCGE) Consortium.

CRediT authorship contribution statement

Reka Lorincz: Data curation, Investigation, Formal analysis, Writing – original draft, Visualization, Project administration. **Aluet B. Alvarez**: Investigation, Project administration. **Chris J. Walkey**: Investigation, Validation, Formal analysis. **Samir A. Mendonça**: Investigation, Formal analysis. **Zhi Hong Lu**: Investigation, Formal analysis. **Alexa E. Martinez**: Investigation, Formal analysis. **Cecilia Ljunberg**: Investigation, Formal analysis. **Jason D Heaney**: Resources, Methology. **William R. Lagor**: Resources, Methology. **David T. Curiel**: Conceptualization, Resources, Writing – review & editing, Supervision, Funding acquisition.

Conflict of interest statement

The authors declare that they have no known competing financial interests or personal relationships that could have appeared to influence the work reported in this paper.

Acknowledgments

We acknowledge the financial support from the National Institute for Health (1UG3TR002851–0). This work was initiated and completed as part of our involvement in the NIH Somatic Cell Genome Editing (SCGE) Consortium.

Appendix A. Supporting information

Supplementary data associated with this article can be found in the online version at doi:10.1016/j.biopha.2022.114189.

References

[1] K. Saha, E.J. Sontheimer, P.J. Brooks, M.R. Dwinell, C.A. Gersbach, D.R. Liu, S. A. Murray, S.Q. Tsai, R.C. Wilson, D.G. Anderson, et al., The NIH Somatic Cell Genome Editing program, Nature 592 (2021) 195–204, https://doi.org/10.1038/s41586-021-03191-1.
[2] S.C. Hurt, P.I. Dickson, D.T. Curiel, Mucopolysaccharidoses type I gene therapy, J. Inherit. Metab. Dis. 44 (2021) 1088–1098, https://doi.org/10.1002/jimd.12414.
[3] C.J. Stephens, E. Kashentseva, W. Everett, L. Kaliberova, D.T. Curiel, Targeted in vivo knock-in of human alpha-1-antitrypsin cDNA using adenoviral delivery of CRISPR/Cas9, Gene Ther. 25 (2018) 139–156, https://doi.org/10.1038/s41434-018-0003-1.
[4] C.J. Stephens, E.J. Lauron, E. Kashentseva, Z.H. Lu, W.M. Yokoyama, D.T. Curiel, Long-term correction of hemophilia B using adenoviral delivery of CRISPR/Cas9, J. Control. Release: Off. J. Control. Release Soc. 298 (2019) 128–141, https://doi.org/10.1016/j.jconrel.2019.02.009.
[5] R. Lorincz, D.T. Curiel, Adv. Alpha-1 Antitrypsin Gene Ther. 63 (2020) 560–570, https://doi.org/10.1165/rcmb.2020-0159PS.
[6] T. VandenDriessche, M.K. Chuah, Targeting endothelial cells by gene therapy, Blood 122 (2013) 1993–1994, https://doi.org/10.1182/blood-2013-08-518266.
[7] W. Wu, Y. Yang, F. Yao, L. Dong, X. Xia, S. Zhang, H. Lei, AAV-mediated in vivo genome editing in vascular endothelial cells, Methods 194 (2021) 12–17, https://doi.org/10.1016/j.ymeth.2020.12.001.
[8] X. Zhang, H. Jin, X. Huang, B. Chaurasiya, D. Dong, T.P. Shanley, Y.-Y. Zhao, Robust genome editing in adult vascular endothelium by nanoparticle delivery of CRISPR-Cas9 plasmid DNA, Cell Rep. (2022) *38*, https://doi.org/10.1016/j.celrep.2021.110196.
[9] Lu, Z.H.; Dmitriev, I.P.; Brough, D.E.; Kashentseva, E.A.; Li, J.; Curiel, D.T. A new gorilla adenoviral vector with natural lung tropism avoids liver toxicity and is

amenable for capsid engineering and vector retargeting, 2020, JVI.00265–00220, doi:10.1128/JVI.00265–20%J Journal of Virology.
[10] Z.H. Lu, S. Kaliberov, J. Zhang, B. Muz, A.K. Azab, R.E. Sohn, L. Kaliberova, Y. Du, D.T. Curiel, J.M. Arbeit, The myeloid-binding peptide adenoviral vector enables multi-organ vascular endothelial gene targeting, Lab. Investig. ; a J. Tech. Methods Pathol. 94 (2014) 881–892, https://doi.org/10.1038/labinvest.2014.78.
[11] O.J. Müller, F. Kaul, M.D. Weitzman, R. Pasqualini, W. Arap, J.A. Kleinschmidt, M. Trepel, Random peptide libraries displayed on adeno-associated virus to select for targeted gene therapy vectors, Nat. Biotechnol. 21 (2003) 1040–1046, https://doi.org/10.1038/nbt856.
[12] M.O. Alberti, J.C. Roth, M. Ismail, Y. Tsuruta, E. Abraham, L. Pereboeva, S. L. Gerson, D.T. Curiel, Derivation of a myeloid cell-binding adenovirus for gene therapy of inflammation, PloS One 7 (2012), e37812, https://doi.org/10.1371/journal.pone.0037812.
[13] J.S. Suk, Q. Xu, N. Kim, J. Hanes, L.M. Ensign, PEGylation as a strategy for improving nanoparticle-based drug and gene delivery, Adv. Drug Deliv. Rev. 99 (2016) 28–51, https://doi.org/10.1016/j.addr.2015.09.012.
[14] X. Song, Y. Cui, Y. Wang, Y. Zhang, Q. He, Z. Yu, C. Xu, H. Ning, Y. Han, Y. Cai, et al., Genome editing with AAV-BR1-CRISPR in postnatal mouse brain endothelial cells, Int J. Biol. Sci. 18 (2022) 652–660, https://doi.org/10.7150/ijbs.64188.
[15] X. Huang, G. Zhou, W. Wu, Y. Duan, G. Ma, J. Song, R. Xiao, L. Vandenberghe, F. Zhang, P.A. D'Amore, et al., Genome editing abrogates angiogenesis in vivo, Nat. Commun. 8 (2017) 112, https://doi.org/10.1038/s41467-017-00140-3.
[16] H.C.J. Ertl, Preclinical models to assess the immunogenicity of AAV vectors, Cell Immunol. 342 (2019), 103722, https://doi.org/10.1016/j.cellimm.2017.11.006.
[17] A. Rossi, A. Salvetti, [Integration of AAV vectors and insertional mutagenesis], Med. Sci.: M/S 32 (2016) 167–174, https://doi.org/10.1051/medsci/20163202010.
[18] K.S. Hanlon, B.P. Kleinstiver, S.P. Garcia, M.P. Zaborowski, A. Volak, S.E. Spirig, A. Muller, A.A. Sousa, S.Q. Tsai, N.E. Bengtsson, et al., High levels of AAV vector integration into CRISPR-induced DNA breaks, Nat. Commun. 10 (2019) 4439, https://doi.org/10.1038/s41467-019-12449-2.
[19] I.P. Dmitriev, S.A. Kaliberov, Targeted Adenoviral Vectors I: Transductional Targeting, Aden Vectors Gene Ther. (2016) 231–257, https://doi.org/10.1016/b978-0-12-800276-6.00009-7.
[20] Y.S. Ahi, D.S. Bangari, S.K. Mittal, Adenoviral vector immunity: its implications and circumvention strategies, Curr. gene Ther. 11 (2011) 307–320, https://doi.org/10.2174/156652311796150372.
[21] A.K. Zaiss, H.B. Machado, H.R. Herschman, The influence of innate and pre-existing immunity on adenovirus therapy, J. Cell Biochem 108 (2009) 778–790, https://doi.org/10.1002/jcb.22328.
[22] H. Fausther-Bovendo, G.P. Kobinger, Pre-existing immunity against Ad vectors: humoral, cellular, and innate response, what's important? Hum. Vaccin Immunother. 10 (2014) 2875–2884, https://doi.org/10.4161/hv.29594.
[23] Z. Xiang, Y. Li, A. Cun, W. Yang, S. Ellenberg, W.M. Switzer, M.L. Kalish, H.C. Ertl, Chimpanzee adenovirus antibodies in humans, sub-Saharan Africa, Emerg. Infect. Dis. 12 (2006) 1596–1599, https://doi.org/10.3201/eid1210.060078.
[24] A.O. Hassan, F. Feldmann, H. Zhao, D.T. Curiel, A. Okumura, T.-L. Tang-Huau, J. B. Case, K. Meade-White, J. Callison, R.E. Chen, et al., A single intranasal dose of chimpanzee adenovirus-vectored vaccine protects against SARS-CoV-2 infection in rhesus macaques, Cell Rep. Med. 2 (2021), 100230, https://doi.org/10.1016/j.xcrm.2021.100230.
[25] A.O. Hassan, N.M. Kafai, I.P. Dmitriev, J.M. Fox, B.K. Smith, I.B. Harvey, R. E. Chen, E.S. Winkler, A.W. Wessel, J.B. Case, et al., A Single-Dose Intranasal ChAd Vaccine Protects Upper and Lower Respiratory Tracts against SARS-CoV-2, e113, Cell 183 (2020) 169–184, https://doi.org/10.1016/j.cell.2020.08.026.
[26] J.A. Fonseca, J.N. McCaffery, E. Kashentseva, B. Singh, I.P. Dmitriev, D.T. Curiel, A. Moreno, A prime-boost immunization regimen based on a simian adenovirus 36 vectored multi-stage malaria vaccine induces protective immunity in mice, Vaccine 35 (2017) 3239–3248, https://doi.org/10.1016/j.vaccine.2017.04.062.
[27] G.P. Kobinger, H. Feldmann, Y. Zhi, G. Schumer, G. Gao, F. Feldmann, S. Jones, J. M. Wilson, Chimpanzee adenovirus vaccine protects against Zaire Ebola virus, Virology 346 (2006) 394–401, https://doi.org/10.1016/j.virol.2005.10.042.
[28] M.O. Alberti, J.S. Deshane, D.D. Chaplin, L. Pereboeva, D.T. Curiel, J.C. Roth, A myeloid cell-binding adenovirus efficiently targets gene transfer to the lung and escapes liver tropism, Gene Ther. 20 (2013) 733–741, https://doi.org/10.1038/gt.2012.91.
[29] T.A. Smith, B.D. White, J.M. Gardner, M. Kaleko, A. McClelland, Transient immunosuppression permits successful repetitive intravenous administration of an adenovirus vector, Gene Ther. 3 (1996) 496–502.
[30] K. Saydaminova, X. Ye, H. Wang, M. Richter, M. Ho, H. Chen, N. Xu, J.-S. Kim, E. Papapetrou, M.C. Holmes, et al., Efficient genome editing in hematopoietic stem cells with helper-dependent Ad5/35 vectors expressing site-specific endonucleases under microRNA regulation, Mol. Ther. - Methods Clin. Dev. 2 (2015), https://doi.org/10.1038/mtm.2014.57.
[31] E.E. Perez, J. Wang, J.C. Miller, Y. Jouvenot, K.A. Kim, O. Liu, N. Wang, G. Lee, V. V. Bartsevich, Y.L. Lee, et al., Establishment of HIV-1 resistance in CD4+ T cells by genome editing using zinc-finger nucleases, Nat. Biotechnol. 26 (2008) 808–816, https://doi.org/10.1038/nbt1410.
[32] M. Gossen, S. Freundlieb, G. Bender, G. Müller, W. Hillen, H. Bujard, Transcriptional activation by tetracyclines in mammalian cells, Sci. (N. Y., N. Y.) 268 (1995) 1766–1769, https://doi.org/10.1126/science.7792603.
[33] L.E. Fry, C.F. Peddle, M. Stevanovic, A.R. Barnard, M.E. McClements, R. E. MacLaren, Promoter orientation within an AAV-CRISPR vector affects Cas9 expression and gene editing efficiency, Crispr J. 3 (2020) 276–283, https://doi.org/10.1089/crispr.2020.0021.
[34] L. Madisen, T.A. Zwingman, S.M. Sunkin, S.W. Oh, H.A. Zariwala, H. Gu, L.L. Ng, R.D. Palmiter, M.J. Hawrylycz, A.R. Jones, et al., A robust and high-throughput Cre reporting and characterization system for the whole mouse brain, Nat. Neurosci. 13 (2010) 133–140, https://doi.org/10.1038/nn.2467.
[35] J. Wang, N. Niu, S. Xu, Z.G. Jin, A simple protocol for isolating mouse lung endothelial cells, Sci. Rep. 9 (2019) 1458, https://doi.org/10.1038/s41598-018-37130-4.
[36] S.J. Dumas, E. Meta, N.V. Conchinha, L. Sokol, R. Chen, M. Borri, L.-A. Teuwen, K. Veys, M. García-Caballero, V. Geldhof, et al., Protocols for endothelial cell isolation from mouse tissues: kidney, spleen, and testis, STAR Protoc. 2 (2021), 100523, https://doi.org/10.1016/j.xpro.2021.100523.
[37] J. Davignon, P. Ganz, Role of endothelial dysfunction in atherosclerosis, Circulation 109 (2004) Iii27–Iii32, https://doi.org/10.1161/01.CIR.0000131515.03336.f8.
[38] R.J. Widmer, A. Lerman, Endothelial dysfunction and cardiovascular disease, Glob. Cardiol. Sci. Pr. 2014 (2014) 291–308, https://doi.org/10.5339/gcsp.2014.43.
[39] R.J. Kelleher, R.L. Soiza, Evidence of endothelial dysfunction in the development of Alzheimer's disease: Is Alzheimer's a vascular disorder? Am. J. Cardiovasc Dis. 3 (2013) 197–226.
[40] M. Couto, V. Coelho-Santos, L. Santos, C. Fontes-Ribeiro, A.P. Silva, C.M.F. Gomes, The interplay between glioblastoma and microglia cells leads to endothelial cell monolayer dysfunction via the interleukin-6-induced JAK2/STAT3 pathway, J. Cell Physiol. 234 (2019) 19750–19760, https://doi.org/10.1002/jcp.28575.
[41] C. Ince, P.R. Mayeux, T. Nguyen, H. Gomez, J.A. Kellum, G.A. Ospina-Tascón, G. Hernandez, P. Murray, D. De Backer, THE ENDOTHELIUM IN SEPSIS, Shock 45 (2016) 259–270, https://doi.org/10.1097/shk.0000000000000473.
[42] A.G. Vassiliou, A. Kotanidou, I. Dimopoulou, S.E. Orfanos, Endothelial damage in acute respiratory distress syndrome, Int J. Mol. Sci. 21 (2020), https://doi.org/10.3390/ijms21228793.
[43] H.M. Otifi, B.K. Adiga, Endothelial Dysfunction in Covid-19 Infection, Am. J. Med Sci. 363 (2022) 281–287, https://doi.org/10.1016/j.amjms.2021.12.010.
[44] A. Barzel, N.K. Paulk, Y. Shi, Y. Huang, K. Chu, F. Zhang, P.N. Valdmanis, L. P. Spector, M.H. Porteus, K.M. Gaensler, et al., Promoterless gene targeting without nucleases ameliorates haemophilia B in mice, Nature 517 (2015) 360–364, https://doi.org/10.1038/nature13864.
[45] J.D. Finn, A.R. Smith, M.C. Patel, L. Shaw, M.R. Youniss, J. van Heteren, T. Dirstine, C. Ciullo, R. Lescarbeau, J. Seitzer, et al., A single administration of CRISPR/Cas9 lipid nanoparticles achieves robust and persistent in vivo genome editing, Cell Rep. 22 (2018) 2227–2235, https://doi.org/10.1016/j.celrep.2018.02.014.
[46] H. Yin, C.-Q. Song, S. Suresh, Q. Wu, S. Walsh, L.H. Rhym, E. Mintzer, M. F. Bolukbasi, L.J. Zhu, K. Kauffman, et al., Structure-guided chemical modification of guide RNA enables potent non-viral in vivo genome editing, Nat. Biotechnol. 35 (2017) 1179–1187, https://doi.org/10.1038/nbt.4005.
[47] M. Buggio, C. Towe, A. Annan, S. Kaliberov, Z.H. Lu, C. Stephens, J.M. Arbeit, D. T. Curiel, Pulmonary vasculature directed adenovirus increases epithelial lining fluid alpha-1 antitrypsin levels, J. Gene Med. 18 (2016) 38–44, https://doi.org/10.1002/jgm.2874.
[48] A.N. Varnavski, R. Calcedo, M. Bove, G. Gao, J.M. Wilson, Evaluation of toxicity from high-dose systemic administration of recombinant adenovirus vector in vector-naïve and pre-immunized mice, Gene Ther. 12 (2005) 427–436, https://doi.org/10.1038/sj.gt.3302347.
[49] Z.H. Lu, J. Li, I.P. Dmitriev, E.A. Kashentseva, D.T. Curiel, Efficient genome editing achieved via plug-and-play adenovirus piggyback transport of Cas9/gRNA complex on viral capsid surface, ACS Nano 16 (2022) 10443–10455, https://doi.org/10.1021/acsnano.2c00909.
[50] S. Roy, Y. Zhi, G.P. Kobinger, J. Figueredo, R. Calcedo, J.R. Miller, H. Feldmann, J. M. Wilson, Generation of an adenoviral vaccine vector based on simian adenovirus 21, J. Gen. Virol. 87 (2006) 2477–2485, https://doi.org/10.1099/vir.0.81989-0.
[51] T. Seki, I. Dmitriev, E. Kashentseva, K. Takayama, M. Rots, K. Suzuki, D.T. Curiel, Artificial extension of the adenovirus fiber shaft inhibits infectivity in coxsackievirus and adenovirus receptor-positive cell lines, J. Virol. 76 (2002) 1100–1108, https://doi.org/10.1128/jvi.76.3.1100-1108.2002.
[52] S. Roy, A. Medina-Jaszek, M.J. Wilson, A. Sandhu, R. Calcedo, J. Lin, J.M. Wilson, Creation of a panel of vectors based on ape adenovirus isolates, J. Gene Med. 13 (2011) 17–25, https://doi.org/10.1002/jgm.1530.
[53] S. Wang, C. Sengel, M.M. Emerson, C.L. Cepko, A gene regulatory network controls the binary fate decision of rod and bipolar cells in the vertebrate retina, Dev. Cell 30 (2014) 513–527, https://doi.org/10.1016/j.devcel.2014.07.018.
[54] M. Tabebordbar, K. Zhu, J.K.W. Cheng, W.L. Chew, J.J. Widrick, W.X. Yan, C. Maesner, E.Y. Wu, R. Xiao, F.A. Ran, et al., In vivo gene editing in dystrophic mouse muscle and muscle stem cells, Sci. (N. Y., N. Y.) 351 (2016) 407–411, https://doi.org/10.1126/science.aad5177.
[55] C. Chartier, E. Degryse, M. Gantzer, A. Dieterle, A. Pavirani, M. Mehtali, Efficient generation of recombinant adenovirus vectors by homologous recombination in Escherichia coli, J. Virol. 70 (1996) 4805–4810, https://doi.org/10.1128/jvi.70.7.4805-4810.1996.
[56] V.N. Krasnykh, G.V. Mikheeva, J.T. Douglas, D.T. Curiel, Generation of recombinant adenovirus vectors with modified fibers for altering viral tropism, J. Virol. 70 (1996) 6839–6846.
[57] C. Mueller, G. Gernoux, A.M. Gruntman, F. Borel, E.P. Reeves, R. Calcedo, F. N. Rouhani, A. Yachnis, M. Humphries, M. Campbell-Thompson, et al., 5 year expression and neutrophil defect repair after gene therapy in Alpha-1 antitrypsin

deficiency, Mol. Ther. 25 (2017) 1387–1394, https://doi.org/10.1016/j.ymthe.2017.03.029.
[58] N. Mittereder, K.L. March, B.C. Trapnell, Evaluation of the concentration and bioactivity of adenovirus vectors for gene therapy, J. Virol. 70 (1996) 7498–7509, https://doi.org/10.1128/jvi.70.11.7498-7509.1996.
[59] R.T. Robertson, S.T. Levine, S.M. Haynes, P. Gutierrez, J.L. Baratta, Z. Tan, K. J. Longmuir, Use of labeled tomato lectin for imaging vasculature structures, Histochem Cell Biol. 143 (2015) 225–234, https://doi.org/10.1007/s00418-014-1301-3.